High-frequency-based features for low and high retina haemorrhage classification

Salim Lahmiri[1,2] ✉

[1]*Department of Electrical Engineering, École de Technologie Supérieure, Montreal, Canada*
[2]*CENPARMI, Concordia University, Montreal, Canada*
✉ *E-mail: salim.lahmiri.1@ens.etsmtl.ca*

Published in Healthcare Technology Letters; Received on 17th August 2016; Revised on 8th October 2016; Accepted on 11th October 2016

Haemorrhages (HAs) presence in fundus images is one of the most important indicators of diabetic retinopathy that causes blindness. In this regard, accurate grading of HAs in fundus images is crucial for appropriate medical treatment. The purpose of this Letter is to assess the relative performance of statistical features obtained with three different multi-resolution analysis (MRA) techniques and fed to support vector machine in grading retinal HAs. Considered MRA techniques are the common discrete wavelet transform (DWT), empirical mode decomposition (EMD), and variational mode decomposition (VMD). The obtained experimental results show that statistical features obtained by EMD, VMD, and DWT, respectively, achieved 88.31% ± 0.0832, 71% ± 0.1782, and 64% ± 0.0949 accuracies. It also outperformed VMD and DWT in terms of sensitivity and specificity. Thus, the EMD-based features are promising for grading retinal HAs.

1. Introduction: Diabetic retinopathy (DR) is a disease that causes blindness; moreover, early and appropriate detection is necessary for better medical treatment. In this regard, several works have proposed automated diagnosis systems of fundus images to assist ophthalmologists in the diagnosis of the disease; either by detecting microaneurysms (MAs) [1–3], exudates [4–6], haemorrhages (HAs) [1, 7, 8], or by vessel segmentation-based approaches [4, 9].

The purpose of this Letter is to compare the ability of three multi-resolution-based techniques in grading HAs in fundus images. In particular, the discrete wavelet transform (DWT) [10], empirical mode decomposition (EMD) [11], and variational mode decomposition (VMD) [12, 13] are employed to analyse fundus image for better characterisation. We rely on grading HAs in fundus images for two reasons. First, they present a serious risk of blindness. Indeed, detecting low-grade HAs is essential for early treatment to avoid blindness. Second, only a limited and related works have paid attention to such issue within the context of DR detection [1, 7, 8].

The contribution of the work follows. First, since multi-resolution analysis (MRA) is appropriate to reveal hidden patterns in textural images, we compare the effectiveness of each MRA approach in tackling the hard problem of retina HA grading. This is the first work to focus on performance of MRA techniques in grading HAs in retina. Indeed, accurate and early detection of low-grade HAs is crucial for appropriate medical treatment to avoid blindness. In this regard, non-adaptive (DWT) and adaptive techniques (EMD and VMD) are considered in our work. Second, the performance of the VMD which is a new MRA technique is employed for the first time to check its effectiveness in grading HAs in retina.

The remaining of our Letter follows. A succinct review of methods is given in Section 2. The classification results are presented in Section 3. Finally, we conclude this Letter and suggest directions for future research in Section 4.

2. Methods: In this Letter, each multi-resolution technique is employed in the first stage to obtain fundus image in high-frequency domain. This is a useful step to highlight biological changes and discontinuities due to the presence of HAs. Then, in order to characterise texture, three statistics are computed to describe distribution of pixels including the mean, third moment, and smoothness. In particular, these statistics are computed only from diagonal frequency component obtained by DWT (high–high-frequency sub-band: HH), first bi-dimensional intrinsic mode function (BIMF), and first VM as they all correspond to high-frequency elements of the original image. The extracted statistical features are given to the support vector machine (SVM) [14] to classify data. For instance, the SVM is employed to grade HAs: low versus high severity. In our Letter, the SVM classifier is chosen for several attractive features. Indeed, it is constructed following statistical learning theory to execute the principle of structural risk minimisation. In addition, it is capable to generalise results when dataset is not large. In addition, it tolerates large dimension sets and imperfect data [15]. The block diagram of the experiments is illustrated in Fig. 1.

2.1. MRA techniques: The DWT [10] uses a predetermined wavelet function to analyse an input image into four sub-bands that characterise it for different orientations: the approximation [low–low (LL)], the horizontal detail (low–high), the vertical detail (high–low), and the diagonal detail sub-band (HH). As a result, the DWT provides horizontal, vertical, and diagonal information about the frequency spectrum of the original input image. The DWT decomposition procedure can be replicated simply by decomposing LL sub-band. In our Letter, popular Daubechies-4 wavelet function is used for image analysis at first, second, and third levels of decomposition. Thus, statistical features used to describe distribution of pixels are computed from HH sub-bands at first, second, and third levels of decomposition: HH1, HH2, and HH3.

The two-dimensional (2D) EMD is a fully adaptive multi-resolution technique employed to partition a signal into an ensemble of IMFs based on a sifting algorithm [11]. For instance, the EMD decomposes an image $f(x, y)$ of size $M \times N$ into a set of n BIMFs. Therefore, the image is represented as follows

$$f(x, y) = \sum_{\ell=1}^{n} \mathrm{BIMF}_1(x, y) + \mathrm{res}(x, y) \tag{1}$$

where BIMF(x, y) represents the image at different scales and res (x, y) is a residue. For simplicity, the number n of desired BIMF is fixed to four to speedup the sifting process.

The goal of the VMD is to breakdown an input signal into k distinct VMs, so as each mode is limited within a bandwidth in spectral domain [12, 13]. Therefore, each mode k is typically compact in the region of a centre pulsation ω_k calculated during decomposition [12, 13]. For example, the 1D signal $\boldsymbol{f}$ is represented by several modes u_k

doi: 10.1049/htl.2016.0067

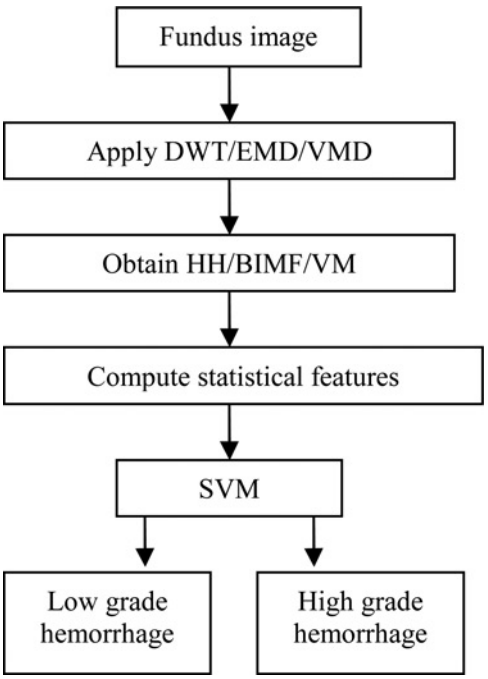

Fig. 1 *Block diagram of experiments*

based on a constrained optimisation problem given by [12]

$$\min_{\boldsymbol{u}_k,\ \boldsymbol{\omega}_k} \left\{ \sum_k \left\| \partial_t \left[\left(\delta(t) + \frac{j}{\pi t} \right) * \boldsymbol{u}_k(t) \right] \mathrm{e}^{-\mathrm{j}\boldsymbol{\omega}_k t} \right\|_2 \right\} \tag{2}$$

Subject to

$$\sum_k \boldsymbol{u}_k = \boldsymbol{f} \tag{3}$$

where $\boldsymbol{f}$ is the signal, u is its mode, ω is the frequency, δ is the Dirac distribution, t is the time script, k is number of modes, and * indicates convolution. The mode u with high-order k indicates low-frequency elements. In the case of an image, the solution to obtain optimal u_k (sub-images) in Fourier domain by using Lagrange multipliers λ is expressed as follows [13]

$$\hat{\boldsymbol{u}}_k = \underset{\hat{\boldsymbol{u}}_k}{\operatorname{argmin}} \left\{ \begin{array}{l} \lambda \left\| \mathrm{j}(\boldsymbol{\omega} - \boldsymbol{\omega}_k) \left[\left(1 + \operatorname{sgn}(\boldsymbol{\omega} \cdot \boldsymbol{\omega}_k)\right) \hat{\boldsymbol{u}}_k(\boldsymbol{\omega}) \right] \right\|_2^2 \\ + \left\| \hat{f}(\boldsymbol{\omega}) - \sum_k \hat{\boldsymbol{u}}_k(\boldsymbol{\omega}) + \dfrac{\hat{\lambda}(\boldsymbol{\omega})}{2} \right\| \end{array} \right\}_2^2 \tag{4}$$

More details are found in [12, 13]. To speedup the VMD algorithm, the parameter k is fixed to four.

Table 1 Average and SD of each feature

MRA	Grade	μ	γ	η
EMD	low	121.55 ± 6.36	0.18 ± 0.05	2.47 ± 2.66
EMD	high	122.02 ± 10.80	0.19 ± 0.01	2.28 ± 4.75
VMD	low	122.98 ± 18.91	0.19 ± 0.01	1.29 ± 7.98
VMD	high	138.73 ± 59.90	0.15 ± 0.07	2.64 ± 8.60
DWT-HH1	low	78.01 ± 6.08	0.14 ± 0.01	14.51 ± 0.61
DWT-HH1	high	78.76 ± 9.73	0.14 ± 0.02	13.89 ± 0.84
DWT-HH2	low	90.56 ± 5.35	0.16 ± 0.01	13.42 ± 0.97
DWT-HH2	high	90.29 ± 7.59	0.16 ± 0.02	13.39 ± 1.51
DWT-HH3	low	102.42 ± 3.54	0.18 ± 0.01	10.65 ± 1.23
DWT-HH3	high	103.31 ± 5.41	0.18 ± 0.01	10.20 ± 1.87

2.2. Features extraction, SVM, and performance measures: In this Letter, three statistical measures are employed to characterise retina texture; namely, the mean (μ), third moment (γ), and smoothness (η) obtained from an image $f(x, y)$ of size $M \times N$. They are given by [16]

$$\mu = \sum_{i=0}^{L-1} z_i p(z_i) \tag{5}$$

$$\gamma = \sum_{i=0}^{L-1} \left(\frac{z_i - \mu}{\delta} \right)^3 \tag{6}$$

$$\eta = \frac{\delta^2}{1 + \delta^2} \tag{7}$$

where

$$\delta = \sum_{i=0}^{L-1} (z_i - \mu)^2 \tag{8}$$

and z is the pixel intensity, p is the probability density of the ith pixel in the histogram, and L is the total number of intensity levels. These extracted statistical features are employed to train the SVM classifier used to distinguish between low- and high-grade HAs.

Technically, the SVM [14] nonlinearly maps the training points to a high-dimensional feature space by employing a kernel function. In particular, a hyper-plane is built to separate data. The nonlinear SVM classifier $S(x)$ for input data $\boldsymbol{x}$ and output data $\boldsymbol{y}$ is given by

$$S(x) = \operatorname{sign}\left(\sum_{i=1} \boldsymbol{y}_i \alpha_i K\langle \boldsymbol{x},\ \boldsymbol{x}_i \rangle + b \right) \tag{9}$$

where α is the Lagrange multiplier, K is a kernel function, and b is a fixed parameter. In this Letter, a polynomial kernel function is employed. Its expression follows

$$K(\boldsymbol{x},\ \boldsymbol{x}_i) = s\left((\boldsymbol{x} \cdot \boldsymbol{x}_i) + 1 \right)^{\mathrm{d}} \tag{10}$$

where d is the polynomial degree fixed to two in our work in order to accelerate convergence of the SVM.

Finally, accuracy, sensitivity, and specificity statistics are employed to assess performance of EMD-SVM, VMD-SVM, HH1-SVM, HH2-SVM, and HH3-SVM models. In our Letter,

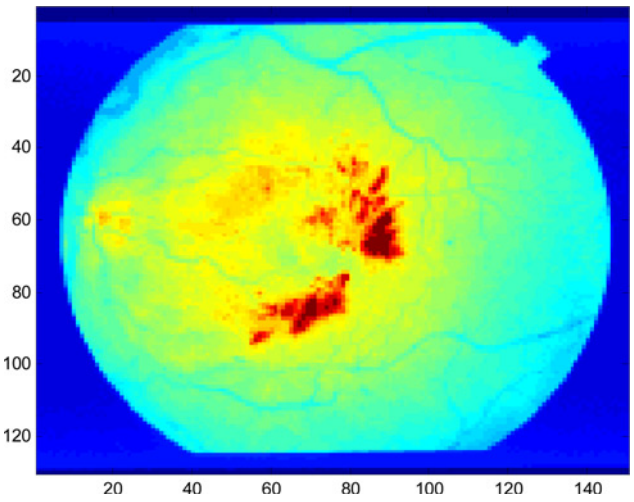

Fig. 2 *Retina image with low-grade HA*

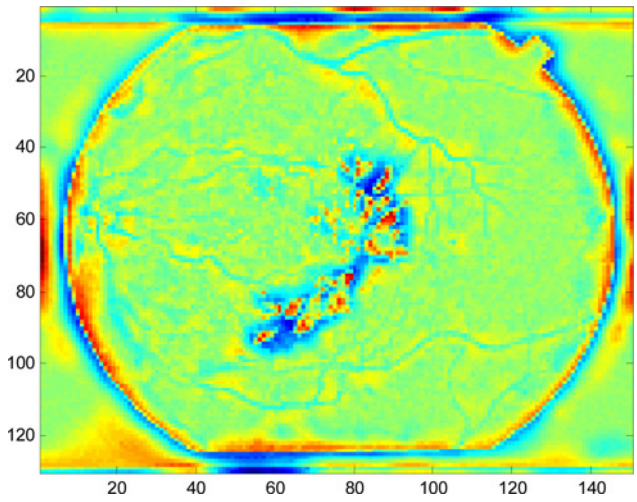

Fig. 3 *Example of first BIMF for low-grade HA*

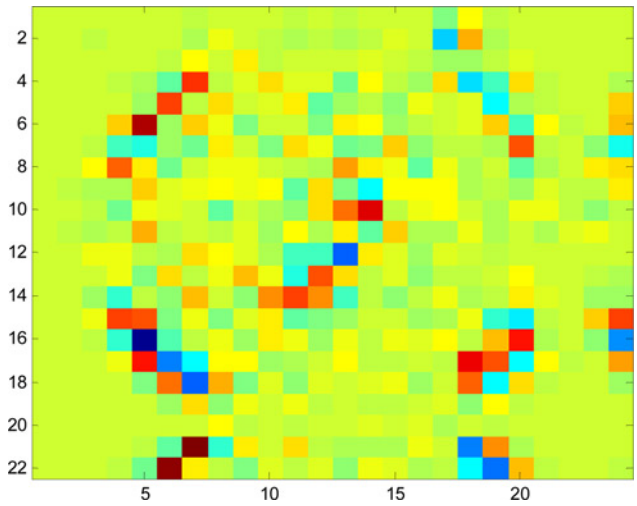

Fig. 5 *Example of DWT resulting HH1 of low-grade HA*

low-grade HAs correspond to positive samples, whilst high-grade HAs correspond to negative samples.

3. Experimental results: We used 24 colour images (150×130 pixels) found in the STructured Analysis of the Retina (STARE) [17] database: 12 low-grade fundus with HAs and 12 fundus images with high-grade HAs. Finally, all experiments are performed with leave-one-out method to better generalise the results as dataset size is small. The experiments are executed on a computer with Intel(R) Core(TM) i5-2500, central processing unit at 3.30 GHz, 4 G random access memory, and MATLAB© 2014. The average and standard deviation (SD) of each feature is provided in Table 1. An example of retina image with low-grade HA is illustrated in Fig. 2. Examples of its high-frequency components obtained by EMD, VMD, and DWT are, respectively, exhibited in Fig. 3–5. Similarly, an example of retina image with high-grade HA is illustrated in Fig. 6, and its resulting high-frequency components obtained by EMD, VMD, and DWT are, respectively, exhibited in Fig. 7–9.

Table 2 summarises the obtained experimental results. For instance, the SVM achieved $88.31\% \pm 0.0832$ accuracy, $83.71\% \pm 0.0983$ sensitivity, and $93.60\% \pm 0.0922$ specificity when it is trained with EMD-based features to distinguish between low- and high-grade retina HAs. Besides, the SVM classifier achieved $71\% \pm 0.1782$ accuracy, $76.03\% \pm 0.1355$ sensitivity, and $66\% \pm 0.2609$ specificity when it is trained with VMD-based features. Finally, the best performance of DWT-based features was achieved by those extracted from HH3 sub-band as the SVM yielded to $64\% \pm 0.0949$ accuracy, $77\% \pm 0.1423$ sensitivity, and $55\% \pm 0.1387$ specificity. Therefore, the EMD-based features performed the best, followed by VMD-based features. Thus, features obtained from standard DWT performed the worst. In particular, the SVM underperformed when trained with DWT-based statistical features for all levels of decompositions. Recall that the highest specificity (correct detection of low-grade retina HAs) is obtained with features extracted from EMD resulting high-frequency image: $83.71\% \pm 0.0983$. This is an interesting result as ophthalmologists are more concerned with detecting low-grade HA with appropriate treatments in order to avoid potential blindness.

As far as we know, this is the first work to compare the performance of several MRA techniques based features in the context of retina HA grading. Three MRA techniques were considered including the classical DWT, the EMD, and the recently introduced VMD. We relied on extracting textural features from MRA domain as the latter is effective in discovering hidden patterns in the original image; especially, sudden changes in biological tissue by focusing on high-frequency components. The DWT was selected as it is conventional but not adaptive. In contrary, the EMD and VMD are adaptive MRA techniques. In addition, while VMD is adaptive, it is also robust to noise that may corrupt the original signal as it is

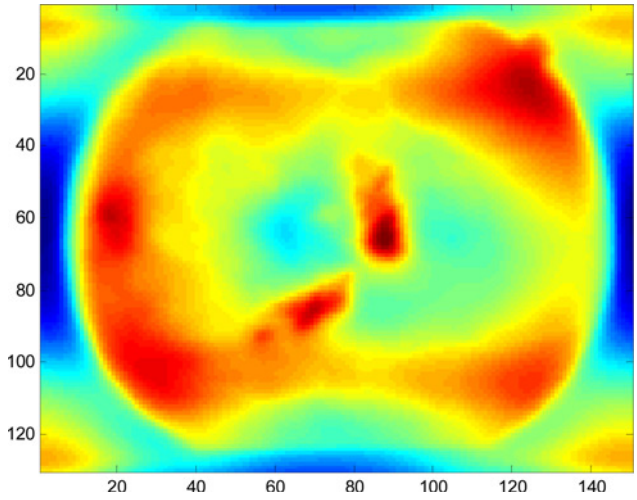

Fig. 4 *Example of first VM for low-grade HA*

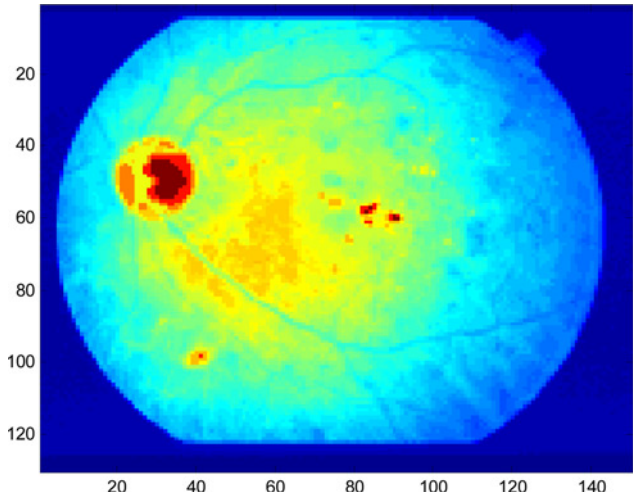

Fig. 6 *Retina image with high-grade HA*

doi: 10.1049/htl.2016.0067

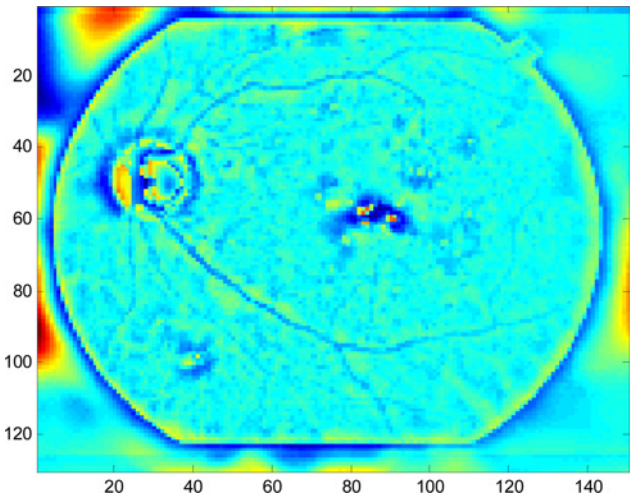

Fig. 7 *Example of first BIMF for high-grade HA*

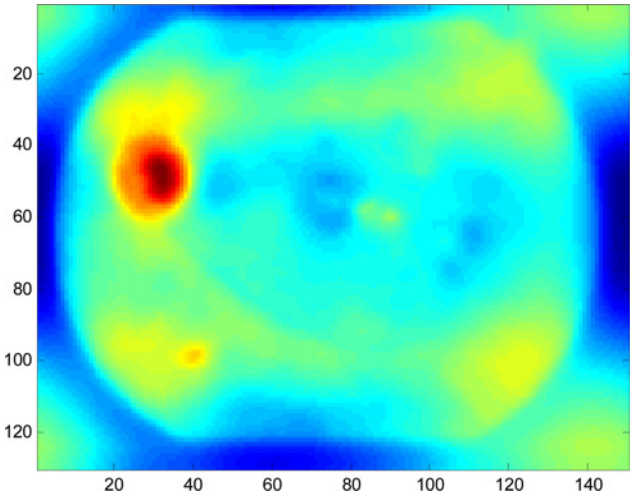

Fig. 8 *Example of first VM for high-grade HA*

based on Wiener filtering in Fourier domain. In fact, EMD and VMD were successful in processing of biomedical signals [18–21]. Besides, though the DWT provides a sparse representation of the original image in frequency domain, it is non-adaptive and

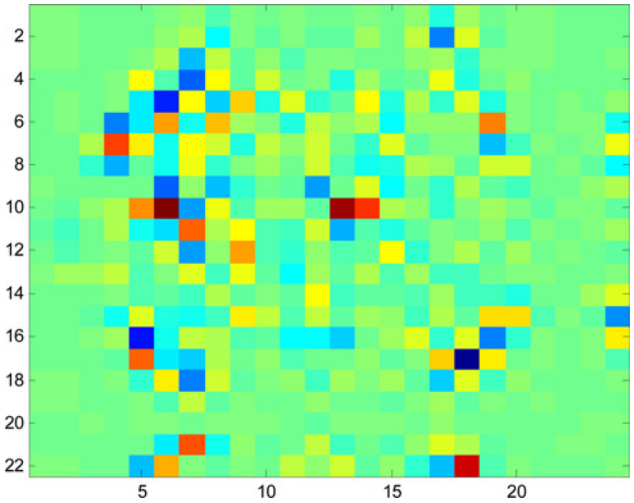

Fig. 9 *Example of DWT resulting HH1 of high-grade HA*

Table 2 Experimental results

Methods	Accuracy	Sensitivity	Specificity
VMD	71% ± 0.1782	76.03% ± 0.1355	66% ± 0.2609
EMD	88.31% ± 0.0832	83.71% ± 0.0983	93.60% ± 0.0922
DWT-HH1	57% ± 0.0609	50% ± 0.1226	65% ± 0.1981
DWT-HH2	59% ± 0.1851	71% ± 0.1485	46% ± 0.2298
DWT-HH3	64% ± 0.0949	77% ± 0.1423	55% ± 0.1387

requires a mother wavelet function to be appropriately determined before image processing. Finally, the SVM was chosen as it is based on structural risk minimisation algorithm. In this regard, it achieves global minimum. Furthermore, it tolerates high-dimensional and/or incomplete data [15]. Indeed, the SVM was found to be effective in biomedical classification problems [5, 6, 22, 23].

Though datasets and experiments are different, the results from some related works [1, 7, 8] are presented for indication purpose. In other words, direct comparison is difficult. For instance, the model in [1] achieved a sensitivity of 84.31 and 87.53% for the recognition of MAs and HAs. In addition, the obtained specificities were 93.63 and 95.08% for MAs and HAs, respectively. In fact, the model was designed to classify spots into MAs and HAs after extracting optic disc, fovea, and retinal tissue, followed by segmentation of dark spot lesions. In a similar problem (distinguishing between MAs and HAs), a sensitivity of 100%, a specificity of 56.00%, and an accuracy of 83.08% were obtained in [7] where a set of regional colour and shape features were extracted, a logistic regression was performed for feature selection, and a radial basis function neural network was employed for classification. Besides, the system designed in [8] achieved an accuracy of 90% in detection of large HAs based on splat feature classification used to distinguish blood splats from non-blood splats. Finally, recall that the authors in [24] only focused on finding optimal DWT sub-band in order to detect DR based on classification of MAs. In our Letter, DWT, EMD, and VMD are all considered and their performances are compared in the context of HA grading: low versus high grade.

4. Conclusion: In summary, we compared the effectiveness of three MRA techniques; namely, the standard DWT, the adaptive EMD, and the new signal processing technique called VMD in grading HAs in fundus images. Indeed, this is the first work to conduct such work. On the basis of our experiments, the main conclusion is that the automatic classification of fundus HAs for evaluation of DR is possible by using EMD-based statistical features and SVM classifier. Indeed, they were found to be promising for grading retinal HAs. Indeed, EMD-based approach is superior to VMD and DWT approaches in terms of accuracy, sensitivity, and specificity. These results indicate that it is helpful in grading retina HA and particularly in detecting low-grade HA to appropriately and early treat them to avoid blindness. For future work, as the results are preliminary in nature, this Letter can be applied to any available database with large number of fundus HA samples. In addition, other classifiers and kernels will be employed for comparison purpose.

5. Funding and declaration of interests: Conflict of interest: none declared.

6 References

[1] Saleh M.D., Eswaran C.: 'An automated decision-support system for non-proliferative diabetic retinopathy disease based on MAs and HAs detection', *Comput. Methods Programs Biomed.*, 2012, **108**, pp. 186–196

[2] Adal K.M., Sidibé D., Ali S., *ET AL.*: 'Automated detection of microaneurysms using scale-adapted blob analysis and semi-supervised learning', *Comput. Methods Programs Biomed.*, 2014, **114**, pp. 1–10
[3] Akram M.U., Khalid S., Khan S.A.: 'Identification and classification of microaneurysms for early detection of diabetic retinopathy', *Pattern Recognit.*, 2013, **46**, pp. 107–116
[4] Youssef D., Solouma N.H.: 'Accurate detection of blood vessels improves the detection of exudates in color fundus images', *Comput. Methods Programs Biomed.*, 2012, **108**, pp. 1052–1061
[5] Lahmiri S., Gargour C., Gabrea M.: 'Automated pathologies detection in retina digital images based on the complex continuous wavelet transform phase angles', *IET Healthc. Technol. Lett.*, 2014, **1**, pp. 104–108
[6] Lahmiri S., Boukadoum M.: 'Automated detection of circinate exudates in retina digital images using empirical mode decomposition and the entropy and uniformity of intrinsic mode functions', *Biomed. Tech./Biomed. Eng.*, 2014, **59**, pp. 357–366
[7] Garcia M., López M.I., Alvarez D D., *ET AL.*: 'Assessment of four neural network based classifiers to automatically detect red lesions in retinal images', *Med. Eng. Phys.*, 2010, **32**, pp. 1085–1093
[8] Tang L., Niemeijer M., Abrilmoff M.D.: 'Splat feature classification: detection of the presence of large retinal hemorrhages'. Proc. IEEE ISBI, 2011, pp. 681–684
[9] Imani E., Javidi M., Pourreza H.-R.: 'Improvement of retinal blood vessel detection using morphological component analysis', *Comput. Methods Programs Biomed.*, 2015, **118**, pp. 263–279
[10] Mallat S.G.: 'Theory for multiresolution signal decomposition: the wavelet representation', *IEEE Trans. Pattern Anal. Mach. Intell.*, 1989, **11**, pp. 674–693
[11] Huang N.E., Shen Z., Long S.R., *ET AL.*: 'The empirical mode decomposition and the Hilbert spectrum for nonlinear and nonstationary time series analysis', *Proc. R. Soc. Lond. A*, 1998, **454**, pp. 903–995
[12] Dragomiretskiy K., Zosso D.: 'Variational mode decomposition', *IEEE Trans. Signal Process.*, 2014, **62**, pp. 531–544
[13] Dragomiretskiy K., Zosso D.: 'Two dimensional variational mode decomposition', in (Eds.): 'Energy minimization methods in computer vision and pattern recognition', 2015, (*LNCS*, **8932**), pp. 197–208
[14] Vapnik V.N.: 'The nature of statistical learning theory' (Springer-Verlag, New York, 1995)
[15] Cristianini N., Shawe-Taylor J.: 'Introduction to support vector machines and other kernel-based learning methods' (Cambridge University Press, Cambridge, UK, 2000)
[16] Gonzalez R.C., Woods R.E., Eddins S.L.: 'Digital image processing using MATLAB' (Prentice-Hall, Upper Saddle River, NJ, 2004)
[17] Available at http://www.ces.clmson.edu/-ahooverlstare/, accessed 22nd September 2014
[18] Lahmiri S.: 'Image denoising in bidimensional empirical mode decomposition domain: the role of student probability distribution function', *IET Healthc. Technol. Lett.*, 2016, **3**, pp. 67–71
[19] Lahmiri S., Boukadoum M.: 'A weighted bio-signal denoising approach using empirical mode decomposition', *Biomed. Eng. Lett.*, 2015, **5**, pp. 131–139
[20] Lahmiri S., Boukadoum M.: 'Physiological signal denoising with variational mode decomposition and weighted reconstruction after DWT thresholding'. Proc. IEEE ISCAS, 2015, pp. 806–809
[21] Lahmiri S.: 'A study of denoising techniques in adaptive multiresolution domains with applications to biomedical images', *IET Healthc. Technol. Lett.*, in press
[22] Lahmiri S., Boukadoum M.: 'New approach for automatic classification of Alzheimer's disease, mild cognitive impairment and healthy brain magnetic resonance images', *IET Healthc. Technol. Lett.*, 2014, **1**, pp. 32–36
[23] Lahmiri S.: 'Image characterization by fractal descriptors in variational mode decomposition domain: application to brain magnetic resonance', *Physica A*, 2016, **456**, pp. 235–243
[24] Quellec G., Lamard M., Josselin P.M., *ET AL.*: 'Optimal wavelet transform for the detection of microaneurysms in retina photographs', *IEEE Trans. Med. Imaging*, 2008, **27**, pp. 1230–1241

doi: 10.1049/htl.2016.0067